

Measurement of the B_s^0 lifetime in the flavor-specific decay channel $B_s^0 \rightarrow D_s^- \mu^+ \nu X$

V.M. Abazov,³¹ B. Abbott,⁶⁷ B.S. Acharya,²⁵ M. Adams,⁴⁶ T. Adams,⁴⁴ J.P. Agnew,⁴¹ G.D. Alexeev,³¹ G. Alkhazov,³⁵ A. Alton^a,⁵⁶ A. Askew,⁴⁴ S. Atkins,⁵⁴ K. Augsten,⁷ C. Avila,⁵ F. Badaud,¹⁰ L. Bagby,⁴⁵ B. Baldin,⁴⁵ D.V. Bandurin,⁷³ S. Banerjee,²⁵ E. Barberis,⁵⁵ P. Baringer,⁵³ J.F. Bartlett,⁴⁵ U. Bassler,¹⁵ V. Bazterra,⁴⁶ A. Bean,⁵³ M. Begalli,² L. Bellantoni,⁴⁵ S.B. Beri,²³ G. Bernardi,¹⁴ R. Bernhard,¹⁹ I. Bertram,³⁹ M. Besançon,¹⁵ R. Beuselinck,⁴⁰ P.C. Bhat,⁴⁵ S. Bhatia,⁵⁸ V. Bhatnagar,²³ G. Blazey,⁴⁷ S. Blessing,⁴⁴ K. Bloom,⁵⁹ A. Boehnlein,⁴⁵ D. Boline,⁶⁴ E.E. Boos,³³ G. Borissov,³⁹ M. Borysova^l,³⁸ A. Brandt,⁷⁰ O. Brandt,²⁰ R. Brock,⁵⁷ A. Bross,⁴⁵ D. Brown,¹⁴ X.B. Bu,⁴⁵ M. Buehler,⁴⁵ V. Buescher,²¹ V. Bunichev,³³ S. Burdin^b,³⁹ C.P. Buszello,³⁷ E. Camacho-Pérez,²⁸ B.C.K. Casey,⁴⁵ H. Castilla-Valdez,²⁸ S. Caughron,⁵⁷ S. Chakrabarti,⁶⁴ K.M. Chan,⁵¹ A. Chandra,⁷² E. Chapon,¹⁵ G. Chen,⁵³ S.W. Cho,²⁷ S. Choi,²⁷ B. Choudhary,²⁴ S. Cihangir,⁴⁵ D. Claes,⁵⁹ J. Clutter,⁵³ M. Cooke^k,⁴⁵ W.E. Cooper,⁴⁵ M. Corcoran,⁷² F. Couderc,¹⁵ M.-C. Cousinou,¹² D. Cutts,⁶⁹ A. Das,⁴² G. Davies,⁴⁰ S.J. de Jong,^{29,30} E. De La Cruz-Burelo,²⁸ F. Déliot,¹⁵ R. Demina,⁶³ D. Denisov,⁴⁵ S.P. Denisov,³⁴ S. Desai,⁴⁵ C. Deterre^c,²⁰ K. DeVaughan,⁵⁹ H.T. Diehl,⁴⁵ M. Diesburg,⁴⁵ P.F. Ding,⁴¹ A. Dominguez,⁵⁹ A. Dubey,²⁴ L.V. Dudko,³³ A. Duperrin,¹² S. Dutt,²³ M. Eads,⁴⁷ D. Edmunds,⁵⁷ J. Ellison,⁴³ V.D. Elvira,⁴⁵ Y. Enari,¹⁴ H. Evans,⁴⁹ V.N. Evdokimov,³⁴ A. Fauré,¹⁵ L. Feng,⁴⁷ T. Ferbel,⁶³ F. Fiedler,²¹ F. Filthaut,^{29,30} W. Fisher,⁵⁷ H.E. Fisk,⁴⁵ M. Fortner,⁴⁷ H. Fox,³⁹ S. Fuess,⁴⁵ P.H. Garbincius,⁴⁵ A. Garcia-Bellido,⁶³ J.A. García-González,²⁸ V. Gavrilov,³² W. Geng,^{12,57} C.E. Gerber,⁴⁶ Y. Gershtein,⁶⁰ G. Ginther,^{45,63} O. Gogota,³⁸ G. Golovanov,³¹ P.D. Grannis,⁶⁴ S. Greder,¹⁶ H. Greenlee,⁴⁵ G. Grenier,¹⁷ Ph. Gris,¹⁰ J.-F. Grivaz,¹³ A. Grohsjean^c,¹⁵ S. Grünendahl,⁴⁵ M.W. Grünewald,²⁶ T. Guillemain,¹³ G. Gutierrez,⁴⁵ P. Gutierrez,⁶⁷ J. Haley,⁶⁸ L. Han,⁴ K. Harder,⁴¹ A. Harel,⁶³ J.M. Hauptman,⁵² J. Hays,⁴⁰ T. Head,⁴¹ T. Hebbeker,¹⁸ D. Hedin,⁴⁷ H. Hegab,⁶⁸ A.P. Heinson,⁴³ U. Heintz,⁶⁹ C. Hensel,¹ I. Heredia-De La Cruz^d,²⁸ K. Herner,⁴⁵ G. Hesketh^f,⁴¹ M.D. Hildreth,⁵¹ R. Hirosky,⁷³ T. Hoang,⁴⁴ J.D. Hobbs,⁶⁴ B. Hoeneisen,⁹ J. Hogan,⁷² M. Hohlfield,²¹ J.L. Holzbauer,⁵⁸ I. Howley,⁷⁰ Z. Hubacek,^{7,15} V. Hynek,⁷ I. Iashvili,⁶² Y. Ilchenko,⁷¹ R. Illingworth,⁴⁵ A.S. Ito,⁴⁵ S. Jabeen^m,⁴⁵ M. Jaffré,¹³ A. Jayasinghe,⁶⁷ M.S. Jeong,²⁷ R. Jesik,⁴⁰ P. Jiang,⁴ K. Johns,⁴² E. Johnson,⁵⁷ M. Johnson,⁴⁵ A. Jonckheere,⁴⁵ P. Jonsson,⁴⁰ J. Joshi,⁴³ A.W. Jung,⁴⁵ A. Juste,³⁶ E. Kajfasz,¹² D. Karmanov,³³ I. Katsanos,⁵⁹ M. Kaur,²³ R. Kehoe,⁷¹ S. Kermiche,¹² N. Khalatyan,⁴⁵ A. Khanov,⁶⁸ A. Kharchilava,⁶² Y.N. Kharzheev,³¹ I. Kiselevich,³² J.M. Kohli,²³ A.V. Kozelov,³⁴ J. Kraus,⁵⁸ A. Kumar,⁶² A. Kupco,⁸ T. Kurča,¹⁷ V.A. Kuzmin,³³ S. Lammers,⁴⁹ P. Lebrun,¹⁷ H.S. Lee,²⁷ S.W. Lee,⁵² W.M. Lee,⁴⁵ X. Lei,⁴² J. Lellouch,¹⁴ D. Li,¹⁴ H. Li,⁷³ L. Li,⁴³ Q.Z. Li,⁴⁵ J.K. Lim,²⁷ D. Lincoln,⁴⁵ J. Linnemann,⁵⁷ V.V. Lipaev,³⁴ R. Lipton,⁴⁵ H. Liu,⁷¹ Y. Liu,⁴ A. Lobodenko,³⁵ M. Lokajicek,⁸ R. Lopes de Sa,⁴⁵ R. Luna-Garcia^g,²⁸ A.L. Lyon,⁴⁵ A.K.A. Maciel,¹ R. Madar,¹⁹ R. Magaña-Villalba,²⁸ S. Malik,⁵⁹ V.L. Malyshev,³¹ J. Mansour,²⁰ J. Martínez-Ortega,²⁸ R. McCarthy,⁶⁴ C.L. McGivern,⁴¹ M.M. Meijer,^{29,30} A. Melnitchouk,⁴⁵ D. Menezes,⁴⁷ P.G. Mercadante,³ M. Merkin,³³ A. Meyer,¹⁸ J. Meyerⁱ,²⁰ F. Miconi,¹⁶ N.K. Mondal,²⁵ M. Mulhearn,⁷³ E. Nagy,¹² M. Narain,⁶⁹ R. Nayyar,⁴² H.A. Neal,⁵⁶ J.P. Negret,⁵ P. Neustroev,³⁵ H.T. Nguyen,⁷³ T. Nunnemann,²² J. Orduna,⁷² N. Osman,¹² J. Osta,⁵¹ A. Pal,⁷⁰ N. Parashar,⁵⁰ V. Parihar,⁶⁹ S.K. Park,²⁷ R. Partridge^e,⁶⁹ N. Parua,⁴⁹ A. Patwa^j,⁶⁵ B. Penning,⁴⁵ M. Perfilov,³³ Y. Peters,⁴¹ K. Petridis,⁴¹ G. Petrillo,⁶³ P. Pétroff,¹³ M.-A. Pleier,⁶⁵ V.M. Podstavkov,⁴⁵ A.V. Popov,³⁴ M. Prewitt,⁷² D. Price,⁴¹ N. Prokopenko,³⁴ J. Qian,⁵⁶ A. Quadt,²⁰ B. Quinn,⁵⁸ P.N. Ratoff,³⁹ I. Razumov,³⁴ I. Ripp-Baudot,¹⁶ F. Rizatdinova,⁶⁸ M. Rominsky,⁴⁵ A. Ross,³⁹ C. Royon,¹⁵ P. Rubinov,⁴⁵ R. Ruchti,⁵¹ G. Sajot,¹¹ A. Sánchez-Hernández,²⁸ M.P. Sanders,²² A.S. Santos^h,¹ G. Savage,⁴⁵ M. Savitskyi,³⁸ L. Sawyer,⁵⁴ T. Scanlon,⁴⁰ R.D. Schamberger,⁶⁴ Y. Scheglov,³⁵ H. Schellman,⁴⁸ C. Schwanenberger,⁴¹ R. Schwienhorst,⁵⁷ J. Sekaric,⁵³ H. Severini,⁶⁷ E. Shabalina,²⁰ V. Shary,¹⁵ S. Shaw,⁴¹ A.A. Shchukin,³⁴ V. Simak,⁷ P. Skubic,⁶⁷ P. Slatery,⁶³ D. Smirnov,⁵¹ G.R. Snow,⁵⁹ J. Snow,⁶⁶ S. Snyder,⁶⁵ S. Söldner-Rembold,⁴¹ L. Sonnenschein,¹⁸ K. Soustruznik,⁶ J. Stark,¹¹ D.A. Stoyanova,³⁴ M. Strauss,⁶⁷ L. Suter,⁴¹ P. Svoisky,⁶⁷ M. Titov,¹⁵ V.V. Tokmenin,³¹ Y.-T. Tsai,⁶³ D. Tsybychev,⁶⁴ B. Tuchming,¹⁵ C. Tully,⁶¹ L. Uvarov,³⁵ S. Uvarov,³⁵ S. Uzunyan,⁴⁷ R. Van Kooten,⁴⁹ W.M. van Leeuwen,²⁹ N. Varelas,⁴⁶ E.W. Varnes,⁴² I.A. Vasilyev,³⁴ A.Y. Verkheev,³¹ L.S. Vertogradov,³¹ M. Verzocchi,⁴⁵ M. Vesterinen,⁴¹ D. Vilanova,¹⁵ P. Vokac,⁷ H.D. Wahl,⁴⁴ M.H.L.S. Wang,⁴⁵ J. Warchol,⁵¹ G. Watts,⁷⁴ M. Wayne,⁵¹ J. Weichert,²¹ L. Welty-Rieger,⁴⁸ M.R.J. Williamsⁿ,⁴⁹ G.W. Wilson,⁵³ M. Wobisch,⁵⁴ D.R. Wood,⁵⁵ T.R. Wyatt,⁴¹ Y. Xie,⁴⁵ R. Yamada,⁴⁵

S. Yang,⁴ T. Yasuda,⁴⁵ Y.A. Yatsunenko,³¹ W. Ye,⁶⁴ Z. Ye,⁴⁵ H. Yin,⁴⁵ K. Yip,⁶⁵ S.W. Youn,⁴⁵ J.M. Yu,⁵⁶
J. Zennaro,⁶² T.G. Zhao,⁴¹ B. Zhou,⁵⁶ J. Zhu,⁵⁶ M. Zielinski,⁶³ D. Zieminska,⁴⁹ and L. Zivkovic¹⁴

(The D0 Collaboration)

¹LAFEX, Centro Brasileiro de Pesquisas Físicas, Rio de Janeiro, Brazil

²Universidade do Estado do Rio de Janeiro, Rio de Janeiro, Brazil

³Universidade Federal do ABC, Santo André, Brazil

⁴University of Science and Technology of China, Hefei, People's Republic of China

⁵Universidad de los Andes, Bogotá, Colombia

⁶Charles University, Faculty of Mathematics and Physics,
Center for Particle Physics, Prague, Czech Republic

⁷Czech Technical University in Prague, Prague, Czech Republic

⁸Institute of Physics, Academy of Sciences of the Czech Republic, Prague, Czech Republic

⁹Universidad San Francisco de Quito, Quito, Ecuador

¹⁰LPC, Université Blaise Pascal, CNRS/IN2P3, Clermont, France

¹¹LPSC, Université Joseph Fourier Grenoble 1, CNRS/IN2P3,
Institut National Polytechnique de Grenoble, Grenoble, France

¹²CPPM, Aix-Marseille Université, CNRS/IN2P3, Marseille, France

¹³LAL, Université Paris-Sud, CNRS/IN2P3, Orsay, France

¹⁴LPNHE, Universités Paris VI and VII, CNRS/IN2P3, Paris, France

¹⁵CEA, Irfu, SPP, Saclay, France

¹⁶IPHC, Université de Strasbourg, CNRS/IN2P3, Strasbourg, France

¹⁷IPNL, Université Lyon 1, CNRS/IN2P3, Villeurbanne, France and Université de Lyon, Lyon, France

¹⁸III. Physikalisches Institut A, RWTH Aachen University, Aachen, Germany

¹⁹Physikalisches Institut, Universität Freiburg, Freiburg, Germany

²⁰II. Physikalisches Institut, Georg-August-Universität Göttingen, Göttingen, Germany

²¹Institut für Physik, Universität Mainz, Mainz, Germany

²²Ludwig-Maximilians-Universität München, München, Germany

²³Panjab University, Chandigarh, India

²⁴Delhi University, Delhi, India

²⁵Tata Institute of Fundamental Research, Mumbai, India

²⁶University College Dublin, Dublin, Ireland

²⁷Korea Detector Laboratory, Korea University, Seoul, Korea

²⁸CINVESTAV, Mexico City, Mexico

²⁹Nikhef, Science Park, Amsterdam, the Netherlands

³⁰Radboud University Nijmegen, Nijmegen, the Netherlands

³¹Joint Institute for Nuclear Research, Dubna, Russia

³²Institute for Theoretical and Experimental Physics, Moscow, Russia

³³Moscow State University, Moscow, Russia

³⁴Institute for High Energy Physics, Protvino, Russia

³⁵Petersburg Nuclear Physics Institute, St. Petersburg, Russia

³⁶Institució Catalana de Recerca i Estudis Avançats (ICREA) and Institut de Física d'Altes Energies (IFAE), Barcelona, Spain

³⁷Uppsala University, Uppsala, Sweden

³⁸Taras Shevchenko National University of Kyiv, Kiev, Ukraine

³⁹Lancaster University, Lancaster LA1 4YB, United Kingdom

⁴⁰Imperial College London, London SW7 2AZ, United Kingdom

⁴¹The University of Manchester, Manchester M13 9PL, United Kingdom

⁴²University of Arizona, Tucson, Arizona 85721, USA

⁴³University of California Riverside, Riverside, California 92521, USA

⁴⁴Florida State University, Tallahassee, Florida 32306, USA

⁴⁵Fermi National Accelerator Laboratory, Batavia, Illinois 60510, USA

⁴⁶University of Illinois at Chicago, Chicago, Illinois 60607, USA

⁴⁷Northern Illinois University, DeKalb, Illinois 60115, USA

⁴⁸Northwestern University, Evanston, Illinois 60208, USA

⁴⁹Indiana University, Bloomington, Indiana 47405, USA

⁵⁰Purdue University Calumet, Hammond, Indiana 46323, USA

⁵¹University of Notre Dame, Notre Dame, Indiana 46556, USA

⁵²Iowa State University, Ames, Iowa 50011, USA

⁵³University of Kansas, Lawrence, Kansas 66045, USA

⁵⁴Louisiana Tech University, Ruston, Louisiana 71272, USA

⁵⁵Northeastern University, Boston, Massachusetts 02115, USA

⁵⁶University of Michigan, Ann Arbor, Michigan 48109, USA

⁵⁷Michigan State University, East Lansing, Michigan 48824, USA

⁵⁸University of Mississippi, University, Mississippi 38677, USA

- ⁵⁹University of Nebraska, Lincoln, Nebraska 68588, USA
⁶⁰Rutgers University, Piscataway, New Jersey 08855, USA
⁶¹Princeton University, Princeton, New Jersey 08544, USA
⁶²State University of New York, Buffalo, New York 14260, USA
⁶³University of Rochester, Rochester, New York 14627, USA
⁶⁴State University of New York, Stony Brook, New York 11794, USA
⁶⁵Brookhaven National Laboratory, Upton, New York 11973, USA
⁶⁶Langston University, Langston, Oklahoma 73050, USA
⁶⁷University of Oklahoma, Norman, Oklahoma 73019, USA
⁶⁸Oklahoma State University, Stillwater, Oklahoma 74078, USA
⁶⁹Brown University, Providence, Rhode Island 02912, USA
⁷⁰University of Texas, Arlington, Texas 76019, USA
⁷¹Southern Methodist University, Dallas, Texas 75275, USA
⁷²Rice University, Houston, Texas 77005, USA
⁷³University of Virginia, Charlottesville, Virginia 22904, USA
⁷⁴University of Washington, Seattle, Washington 98195, USA
(Dated: October 6, 2014)

We present an updated measurement of the B_s^0 lifetime from the D0 collaboration using the semileptonic decays $B_s^0 \rightarrow D_s^- \mu^+ \nu X$, with $D_s^- \rightarrow \phi \pi^-$ and $\phi \rightarrow K^+ K^-$ (and the charge conjugate process). This measurement uses the full Tevatron Run II sample of proton-antiproton collisions at $\sqrt{s} = 1.96$ TeV, comprising an integrated luminosity of 10.4 fb^{-1} . We find a flavor-specific lifetime $\tau_{\text{fs}}(B_s^0) = 1.479 \pm 0.010 \text{ (stat)} \pm 0.021 \text{ (syst)} \text{ ps}$. This technique is also used to determine the B^0 lifetime using the analogous $B^0 \rightarrow D^- \mu^+ \nu X$ decay with $D^- \rightarrow \phi \pi^-$, yielding $\tau(B^0) = 1.534 \pm 0.019 \text{ (stat)} \pm 0.021 \text{ (syst)} \text{ ps}$. Both measurements are consistent with the current world averages, and the B_s^0 lifetime measurement is one of the most precise to date. Taking advantage of the cancellation of systematic uncertainties, we determine the lifetime ratio $\tau_{\text{fs}}(B_s^0)/\tau(B^0) = 0.964 \pm 0.013 \text{ (stat)} \pm 0.007 \text{ (syst)}$.

PACS numbers: 13.20.He, 14.40.Nd

The decays of hadrons containing a b quark are dominated by the weak interaction of the b quark whereas the lighter quarks in the hadron act largely as spectators. In first-order calculations, the decay widths of these hadrons are independent of the flavor of the accompanying light quark(s). Higher-order predictions break this symmetry, with the spectator quarks having roles in the time evolution of the B hadron decay [1, 2]. The flavor dependence leads to an expected lifetime hierarchy of $\tau(B_c) < \tau(\Lambda_b) < \tau(B_s^0) \approx \tau(B^0) < \tau(B^+)$, which has been observed experimentally [3]. The ratios of the lifetimes of different b hadrons are precisely predicted by heavy quark effective theories and provide a way to experimentally study these higher-order effects. Existing measurements are in excellent agreement with predictions [3] for the lifetime ratio $\tau(B^+)/\tau(B^0)$, but until recently the experimental precision has been insufficient to test the corresponding theoretical prediction for $\tau(B_s^0)/\tau(B^0)$. In particular, predictions using inputs from unquenched lattice QCD calculations give $0.996 < \tau(B_s^0)/\tau(B^0) < 1$ [2]. More precise measurements of both B_s^0 lifetime and the ratio to its lighter counterparts are needed to test and refine the models.

A flavor-specific final state such as $B_s^0 \rightarrow D_s^- \mu^+ \nu$ is one where the charge signs of the decay products can be used to know whether the meson was a B_s^0 or \bar{B}_s^0 at the time of decay. As a consequence of neutral B meson flavor oscillations, the B_s^0 lifetime as measured

in semileptonic decays is actually a combination of the lifetimes of the heavy and light mass eigenstates with an equal mixture of these two states at time $t = 0$. If the resulting superposition of two exponential distributions is fitted with a single exponential function, one obtains to second order [4]:

$$\tau_{\text{fs}}(B_s^0) = \frac{1}{\Gamma_s} \cdot \frac{1 + (\Delta\Gamma_s/2\Gamma_s)^2}{1 - (\Delta\Gamma_s/2\Gamma_s)^2}, \quad (1)$$

where $\Gamma_s = (\Gamma_{sL} + \Gamma_{sH})/2$ is the average decay width of the light and heavy states, and $\Delta\Gamma_s$ is the difference $\Gamma_{sL} - \Gamma_{sH}$. This dependence makes the flavor-specific lifetime an important parameter in global fits [5] used to extract $\Delta\Gamma_s$, and hence to constrain possible CP violation in the mixing and interference of B_s^0 mesons.

Previous measurements have been performed by both the CDF [6] and D0 [7] Collaborations, with additional earlier measurements from LEP [8], and CDF [9]. The LHCb Collaboration has also made several measurements of the flavor-specific lifetime of the B_s^0 [10, 11]. During Run II of the Tevatron collider from 2002–2011, the D0 detector [13] accumulated 10.4 fb^{-1} of $p\bar{p}$ collisions at a center-of-mass energy of 1.96 TeV. Using this full dataset, we present the most precise measurement of the B_s^0 lifetime, using the flavor-specific decay $B_s^0 \rightarrow D_s^- \mu^+ \nu X$, with $D_s^- \rightarrow \phi \pi^-$ and $\phi \rightarrow K^+ K^-$ [12]. This supersedes previous measurements made by the D0 Collaboration [7].

A detailed description of the D0 detector can be found elsewhere [13]. The data for this analysis were collected with single muon trigger requirements. Events that only satisfy triggers with track impact parameter (IP) conditions are removed to prevent lifetime biases. Events are considered for selection if they contain a muon candidate identified through signatures both inside and outside the toroid magnet [13]. The muon must be associated with a central track, have transverse momentum (p_T) exceeding 2.0 GeV/ c , and a total momentum of $p > 3.0$ GeV/ c . For events satisfying the muon requirements, candidate $B_s^0 \rightarrow D_s^- \mu^+ \nu X$ decays are reconstructed by first combining two charged particle tracks of opposite charge, which are assigned the charged kaon mass. Both tracks must satisfy $p_T > 1.0$ GeV/ c , and the invariant mass of the two-kaon system must be consistent with a ϕ meson decay, $1.008 \text{ GeV}/c^2 < M(K^+ K^-) < 1.032 \text{ GeV}/c^2$. This ϕ candidate is then combined with a third track, assigned the charged pion mass, to form a $D_s^- \rightarrow \phi \pi^-$ candidate. The pion candidate must have $p_T > 0.7$ GeV/ c , and the invariant mass of the $\phi \pi^-$ system must lie within a window that includes the D_s^- meson, $1.73 \text{ GeV}/c^2 < M(\phi \pi^-) < 2.18 \text{ GeV}/c^2$. The combinatorial background is reduced by requiring that the three tracks create a common D_s^- vertex as described in Ref. [14]. Lastly, each D_s^- meson candidate is combined with the muon to reconstruct a B_s^0 meson candidate. The invariant mass must be within the range $3 \text{ GeV}/c^2 < M(D_s^- \mu^+) < 5 \text{ GeV}/c^2$. All four tracks must be associated with the same $p\bar{p}$ interaction vertex (PV), and have hits in the silicon and fiber tracking detectors.

Muon and pion tracks from genuine B_s^0 meson decays must have opposite charge, which defines the right-sign sample. The wrong-sign sample, where they have the same charge, is also retained to help constrain the background model. In the right-sign sample, the reconstructed D_s^- meson is required to be displaced from the PV in the same direction as its momentum in order to reduce combinatoric background.

The flavor-specific B_s^0 lifetime ($\tau(B_s^0)$) can be related to the decay kinematics in the transverse plane,

$$c\tau(B_s^0) = L_{xy} \frac{M}{p_T(B_s^0)}, \quad (2)$$

where M is the B_s^0 mass, taken as the world average [3], and $L_{xy} = \vec{X} \cdot \vec{p}_T / |\vec{p}_T|$ is the transverse decay length, where \vec{X} is the displacement vector from the PV to the secondary vertex in the transverse plane. Since the neutrino is not detected, and the soft hadrons and photons from decays of excited charmed states are not explicitly included in the reconstruction, the p_T of the B_s^0 meson cannot be fully reconstructed. Instead, we use the combined p_T of the muon and D_s^- meson, $p_T(D_s^- \mu^+)$. The reconstructed parameter is the pseudo-proper decay length (PPDL):

$$\text{PPDL} = L_{xy} \frac{M}{p_T(D_s^- \mu^+)}. \quad (3)$$

To model the effect of the missing p_T when the B_s^0 lifetime is extracted from the PPDL distribution, a correction factor K is introduced, defined by:

$$K = \frac{p_T(D_s^- \mu^+)}{p_T(B_s^0)}. \quad (4)$$

The K -factor correction is a probability density function, relating the observed PPDL with the proper decay length, $c\tau = K \cdot \text{PPDL}$. It accounts for the effects of momentum resolution and of any unreconstructed decay products. It is extracted from a Monte Carlo (MC) simulation, separately for a number of specific decays comprising both signal and background components.

MC samples are produced using the PYTHIA event generator [15] to model the production and hadronization phase, interfaced with EVTGEN [16] to model the decays of long-lived hadrons containing b or c quarks. The events are passed through a detailed GEANT simulation of the detector [17] and additional algorithms to reproduce the effects of digitization, detector noise, and pile-up. To ensure that the simulation fully describes the data, and in particular to account for the effect of muon triggers, we reweight the MC events to reproduce the muon transverse momentum distribution observed in data. All selection cuts described above are applied to the simulated events.

Decay channel	Contribution
$D_s^- \mu^+ \nu_\mu$	$(27.5 \pm 2.4)\%$
$D_s^{*-} \mu^+ \nu_\mu \times (D_s^{*-} \rightarrow D_s^- \gamma / D_s^- \pi^0)$	$(66.2 \pm 4.4)\%$
$D_{s(J)}^{*-} \mu^+ \nu_\mu \times (D_{s(J)}^{*-} \rightarrow D_s^{*-} \pi^0 / D_s^- \gamma)$	$(0.4 \pm 5.3)\%$
$D_s^{(*)-} \tau^+ \nu_\tau \times (\tau^+ \rightarrow \mu^+ \bar{\nu}_\mu \nu_\tau)$	$(5.9 \pm 2.7)\%$

TABLE I. Relative contributions to the $D_s^- \mu^+$ signal from different semileptonic B_s^0 decays. The uncertainties are dominated by limited knowledge of the branching fractions [3, 16]. In total, these processes comprise $(80.5 \pm 2.1)\%$ of the events in the $D_s^- \mu^+$ mass broad peak after subtracting combinatorial background.

Table I summarizes the semileptonic B_s^0 decays that contribute to the $D_s^- \mu^+$ signal. Experimentally these processes differ only in the varying amount of energy lost to missing decay products, which is reflected in the final K -factor distribution. Table II shows the list of non-negligible processes from subsequent semileptonic charm decays which also contribute to the signal. These two tables represent the sample composition of the $D_s^- \mu^+$ signal.

We partition the dataset into five data-collection periods, separated by accelerator shutdowns, each comprising 1–3 fb $^{-1}$ of integrated luminosity, to better take into

Decay channel	Contribution
$B^+ \rightarrow D_s^- DX$	$(3.81 \pm 0.75)\%$
$B^0 \rightarrow D_s^- DX$	$(4.13 \pm 0.70)\%$
$B_s^0 \rightarrow D_s^- D_s^{(*)} X$	$(1.11 \pm 0.36)\%$
$B_s^0 \rightarrow D_s^- DX$	$(0.92 \pm 0.44)\%$
$c\bar{c} \rightarrow D_s^- \mu^+$	$(9.53 \pm 1.65)\%$

TABLE II. Other semileptonic decays contributing to the $D_s^- \mu^+$ signal. Listed contributions are obtained after subtracting combinatorial background. The uncertainties are dominated by limited knowledge of the branching fractions [3, 16].

account time- or luminosity-dependent effects. The behavior and overall contribution of the dominant combinatorial backgrounds changed as the collider, detector, and trigger conditions evolved over the course of the Tevatron Run II. Figure 1 shows the $M(\phi\pi^-)$ invariant mass distribution for the right-sign $D_s^- \mu^+$ candidates for one of these data periods. The lifetime is extracted separately for each period and, when including the systematic uncertainties these lifetimes are consistent within the measured uncertainties. The five independent measurements are combined in a weighted average to derive the final lifetime measurement. The MC reweighting as a function of p_T is performed separately for each of the five data samples. The K factors are extracted independently in each sample, with significant shifts observed due to the changing trigger conditions. The K -factor distribution peaks at ≈ 0.9 for the D_s^- signal and at ≈ 0.8 for the first four backgrounds listed in Table II. The K -factor distribution populates $0.5 < K < 1$ for both the signal and background components.

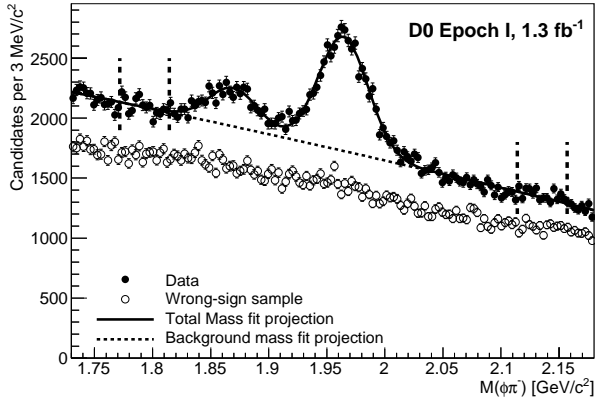


FIG. 1. Distributions of the invariant mass $M(\phi\pi^-)$ for $D_s^- \mu^+$ candidates passing all selection criteria in one of the five data periods. The higher-mass peak is the D_s^- signal, with a smaller D^- peak at lower mass. Sidebands for right-sign sample are indicated with dashed lines and the corresponding distribution for the wrong-sign sample is also shown.

To determine the number of events in the signal re-

gion and define the signal and background samples, we fit a model to the $M(\phi\pi^-)$ invariant mass distribution as shown in Fig. 1. The D_s^- and D^- mass peaks are each modeled using an independent Gaussian distribution to represent the detector mass resolution, and a second-order polynomial is used to model the combinatorial background. Using the information obtained from these fits, we define the signal sample (SS) as those events in the $M(\phi\pi^-)$ mass distribution that are within $\pm 2\sigma$ of the fitted mean D_s^- meson mass, where σ is the Gaussian width of the D_s^- mass peak obtained from the fit. We find a total of 72028 ± 727 $D_s^- \mu^+$ signal candidates in the full dataset. The background sample (BS) includes those events in the sidebands of the D_s^- mass distribution given by -9σ to -7σ and $+7\sigma$ to $+9\sigma$ from the fitted mean mass. Wrong-sign events in the full $M(\phi\pi^-)$ range are also included in the background sample, yielding more events to constrain the behavior of the combinatorial background.

The extraction of the flavor-specific B_s^0 lifetime is performed using an unbinned maximum likelihood fit to the data, based on the PPDL of each candidate [18]. The effects of finite L_{xy} resolution of the detector and the K factors are included in this fit to relate the underlying decay time of the candidates to the corresponding observed quantity. The signal and background samples defined above are fitted simultaneously, with a single shared set of parameters used to model the combinatoric background shape. To validate the lifetime measurement method, we perform a simultaneous fit of the B^0 lifetime using the Cabibbo suppressed decay $B^0 \rightarrow D^- \mu^+ X$ seen in Fig. 1 at lower masses. This measurement also enables the ratio $\tau_{\text{fs}}(B_s^0)/\tau(B^0)$ to be measured with high precision, since the dominant systematic uncertainties are highly correlated between the two lifetime measurements. For simplicity, the details of the fitting function are illustrated for the B_s^0 lifetime fit alone. In practice an additional likelihood product is included to extract the B^0 lifetime in an identical manner.

The likelihood function \mathcal{L} is defined as

$$\mathcal{L} = \prod_{i \in SS} [f_{D_s \mu} \mathcal{F}_{D_s \mu}^i + (1 - f_{D_s \mu}) \mathcal{F}_{\text{comb}}^i] \prod_{j \in BS} \mathcal{F}_{\text{comb}}^j, \quad (5)$$

where $f_{D_s \mu}$ is the fraction of $D_s^- \mu^+$ candidate events in the signal sample, obtained from the fit of the D_s^- mass distribution, and $\mathcal{F}_{D_s \mu}^i$ is the candidate (combinatoric background) probability density function (PDF) evaluated for the i^{th} event. The probability density $\mathcal{F}_{D_s \mu}^i$ is given by

$$\mathcal{F}_{D_s \mu}^i = f_{\bar{c}c} F_{\bar{c}c}^i + f_{B1} F_{B1}^i + f_{B2} F_{B2}^i + f_{B3} F_{B3}^i + f_{B4} F_{B4}^i + \left(1 - f_{\bar{c}c} - f_{B1} - f_{B2} - f_{B3} - f_{B4}\right) F_s^i. \quad (6)$$

Each factor f_X is the expected fraction of a particular component X in the signal sample, obtained from MC

and listed in Tables I and II. The first term accounts for the prompt $c\bar{c}$ component, and the decays $B1$ – $B4$ represent the first four components listed in Table II. The last term of the sum in Eq. (6) represents the signal events $S \equiv (B_s^0 \rightarrow D_s^- \mu^+ \nu X)$ listed in Table I. The factor $F_{\bar{c}c}$ is the lifetime PDF for the $\bar{c}c$ events, given by a Gaussian distribution with a mean of zero and a free width. Each B decay mode is associated with a separate PDF, F_X , modeling the PPDL distribution, given by an exponential decay convoluted with a resolution function and with the K -factor distribution. All B -meson decays are subject to the same PPDL resolution function. A double-Gaussian distribution is used for the resolution function, with widths given by the event-by-event PPDL uncertainty determined from the B_s^0 candidate vertex fit multiplied by two overall scale factors and a ratio between their contributions that are all allowed to vary in the fit.

The combinatoric background PDF, $\mathcal{F}_{\text{comb}}$, is chosen empirically to provide a good fit to the combinatorial background PPDL distribution. It is defined as the sum of the double-Gaussian resolution function and two exponential decay functions for both the positive and negative PPDL regions. The shorter-lived exponential decays are fixed to have the same slope for positive and negative regions, while different slopes are allowed for the longer-lived exponential decays. The fitting was performed using the MINUIT [19] fitting program included in the ROOFIT [20] package. Figure 2 shows the PPDL distribution for the signal sample, along with the projection of the fit model, for one of the five data periods. Table III shows fit results for each data period.

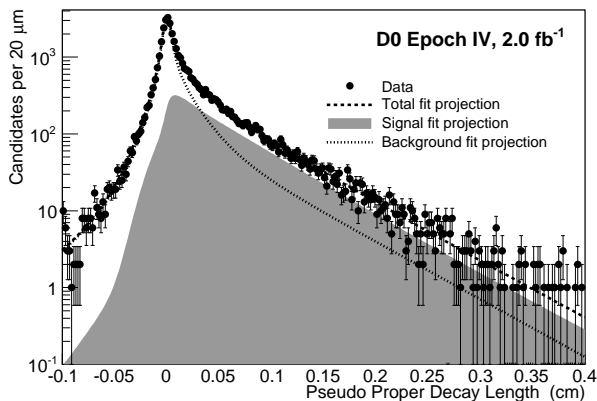


FIG. 2. PPDL distribution for $D_s^- \mu^+$ candidates in the signal sample for one of the five data periods. The projections of the lifetime fitting model, the background function, and the signal function are superimposed.

Using this procedure, the flavor-specific B_s^0 meson lifetime is measured to be $c\tau(B_s^0) = 443.3 \pm 2.9 \mu\text{m}$ (stat). The corresponding B^0 lifetime measurement uses exactly the same procedure for events in the D^- mass

Epoch	$N(D_s)$	$c\tau$ (μm)	$L(f\text{b}^{-1})$
I	17059 ± 399	463.0 ± 6.1	1.3
II	12066 ± 304	445.8 ± 7.1	1.5
III	20574 ± 345	430.3 ± 5.3	3.3
IV	11207 ± 257	445.2 ± 7.3	2.0
V	11122 ± 303	432.6 ± 7.5	2.3
Total/Average	72028 ± 727	443.3 ± 2.9	10.4

TABLE III. Maximum-Likelihood fit results for each data taking period. Only statistical errors are shown.

peak, including a calculation of dedicated K factors and background contributions from semileptonic decays. After combining the results for all five data periods in a weighted average, the final measured lifetime is $c\tau(B^0) = 459.8 \pm 5.6 \mu\text{m}$ (stat), which is in good agreement with the world average of $455.4 \pm 2.1 \mu\text{m}$ [3].

The lifetime fitting procedure is tested using MC pseudo-experiments, in which the generated $B_{(s)}^0$ lifetime is set to a range of different values, and the full fit performed on the simulated data. Good agreement is found between the input and extracted lifetimes in all cases. As an additional cross-check, the data are divided into pairs of sub-samples, and the fit is performed separately for both samples. The divisions correspond to low and high $p_T(B_{(s)}^0)$, central and forward $|\eta(B_{(s)}^0)|$ regions, and $B_{(s)}^0$ versus $\bar{B}_{(s)}^0$ decays. In all cases the measured lifetimes are consistent within uncertainties.

To evaluate systematic uncertainties on the measurements of $c\tau(B_s^0)$, $c\tau(B^0)$, and the ratio $\tau_{\text{fs}}(B_s^0)/\tau(B^0)$, we consider the following possible sources: modelling of the decay length resolution, combinatorial background evaluation, K -factor determination, background contribution from charm semileptonic decays, signal fraction, and alignment of the detector. All other sources investigated are found to be negligible. The effect of possible mismodelling of the decay length resolution is tested by repeating the lifetime fit with alternative resolution models, using a single Gaussian component. A systematic uncertainty is assigned based on the shift in the measured lifetime. We repeat the fit using different combinatorial background samples using only the sideband data or only the wrong-sign sample. The maximum deviation from the central lifetime measurement is assigned as a systematic uncertainty. To determine the effect of uncertainties on the K factors for the signal events, the fractions of the different components are varied within their uncertainties given in Table I. We also recalculate the K factors using different MC decay models [16] leading to a harder p_T distribution of the generated B hadrons. The fraction of each component from semileptonic decays is varied within its uncertainties, and the shift in the measured lifetime is used to assign a systematic uncertainty. The signal fraction parameter, $f_{D_s\mu}$, is fixed for each mass fit performed. We vary this parameter within its statistical and systematic uncertainty, obtained from fit variations

to the background and signal model of the mass PDFs, and assign the observed deviation as the uncertainty arising from this source. Finally, to assess the effect of possible detector mis-alignment, a single MC sample is passed through two different reconstruction algorithms, corresponding to the nominal detector alignment and an alternative model with tracking detector elements shifted spatially within their uncertainties. The observed change in the lifetime is taken as systematic uncertainty due to alignment.

Table IV lists the contributions to the systematic uncertainty from all sources considered. The most significant effect comes from the combinatorial background determination. The total uncertainties on the lifetimes, determined by adding individual components in quadrature, are $6.3 \mu\text{m}$ and $6.4 \mu\text{m}$ for B_s^0 and B^0 mesons, respectively. Correlations in the systematic uncertainties for the B_s^0 and B^0 meson lifetimes are taken into account when evaluating the effect on the lifetime ratio, where the K factor determination dominates.

Uncertainty Source	$\Delta(c\tau_{B_s^0})\mu\text{m}$	$\Delta(c\tau_{B^0})\mu\text{m}$	ΔR
Resolution	0.7	2.1	0.003
Combinatorial Background	5.0	4.9	0.001
K factor	1.6	1.3	0.006
Semileptonic Components	2.6	2.0	0.001
Signal Fraction	1.0	1.8	0.002
Alignment of the detector	2.0	2.0	0.000
Total	6.3	6.4	0.007

TABLE IV. Summary of systematic uncertainty contributions to the B_s^0 and B^0 lifetimes, and to the ratio $R \equiv \tau_{\text{fs}}(B_s^0)/\tau(B^0)$.

Taking all systematic uncertainties into account, the measured lifetime of the B_s^0 meson is determined to be

$$\begin{aligned} c\tau_{\text{fs}}(B_s^0) &= 443.3 \pm 2.9 \text{ (stat)} \pm 6.3 \text{ (syst)} \mu\text{m}, \\ \tau_{\text{fs}}(B_s^0) &= 1.479 \pm 0.010 \text{ (stat)} \pm 0.021 \text{ (syst)} \text{ ps} \\ &= 1.479 \pm 0.023 \text{ (tot)} \text{ ps}, \end{aligned} \quad (7)$$

which is consistent with the current world average of $1.465 \pm 0.031 \text{ ps}$ [3, 5]. The uncertainty in this measurement is dominated by systematic effects. The B^0 lifetime in the corresponding semileptonic decay $B^0 \rightarrow D^- \mu^+ \nu X$ is measured to be

$$\begin{aligned} c\tau(B^0) &= 459.8 \pm 5.6 \text{ (stat)} \pm 6.4 \text{ (syst)} \mu\text{m}, \\ \tau(B^0) &= 1.534 \pm 0.019 \text{ (stat)} \pm 0.021 \text{ (syst)} \text{ ps}. \end{aligned} \quad (8)$$

Taking the world average of $c\tau(B^0) = 455.4 \pm 1.5 \mu\text{m}$ and this measurement of $c\tau_{\text{fs}}(B_s^0)$, we compute the ratio

$$\frac{\tau_{\text{fs}}(B_s^0)}{\tau(B^0)} = 0.973 \pm 0.015, \quad (9)$$

where no correlations have been assumed. Using both lifetimes obtained in the current analysis, the ratio is

determined to be

$$\frac{\tau_{\text{fs}}(B_s^0)}{\tau(B^0)} = 0.964 \pm 0.013 \text{ (stat)} \pm 0.007 \text{ (syst)}. \quad (10)$$

Both results are in reasonable agreement with theoretical predictions from lattice QCD [1, 2], the flavor-specific lifetime has a better precision than the current world average [3, 5], and can be compared to the slightly more precise recent measurement from the LHCb Collaboration [11].

In summary, using 10.4 fb^{-1} of integrated luminosity collected with the D0 detector, we measure the B_s^0 lifetime in the inclusive semileptonic channel $B_s^0 \rightarrow D_s^- \mu^+ \nu X$. We obtain one of the most precise determinations of the flavor-specific B_s^0 lifetime and the corresponding ratio $\tau_{\text{fs}}(B_s^0)/\tau(B^0)$ that can be used to test and refine theoretical QCD predictions.

We thank the staffs at Fermilab and collaborating institutions, and acknowledge support from the DOE and NSF (USA); CEA and CNRS/IN2P3 (France); MON, NRC KI and RFBR (Russia); CNPq, FAPERJ, FAPESP and FUNDUNESP (Brazil); DAE and DST (India); Colciencias (Colombia); CONACyT (Mexico); NRF (Korea); FOM (The Netherlands); STFC and the Royal Society (United Kingdom); MSMT and GACR (Czech Republic); BMBF and DFG (Germany); SFI (Ireland); The Swedish Research Council (Sweden); and CAS and CNSF (China).

-
- [1] D. Becirevic, PoS HEP **2001**, 098 (2001); M. Neubert and C.T. Sachrajda, Nucl. Phys. B **483**, 339 (1997).
 - [2] A. Lenz and U. Nierste, J. High Energy Phys. **06**, 072 (2007) (and recent update arXiv:1102.4274 [hep-ph]).
 - [3] K.A. Olive *et al.* (Particle Data Group), Chin. Phys. C **38**, 090001 (2014).
 - [4] K. Hartkorn and H.-G. Moser, Eur. Phys. J. **C8**, 381 (1999).
 - [5] Y. Amhis *et al.* (Heavy Flavor Averaging Group Collaboration), arXiv:1207.1158 [hep-ex], with web update at http://www.slac.stanford.edu/xorg/hfag/osc/PDG_2014/.
 - [6] T. Aaltonen *et al.* (CDF Collaboration), Phys. Rev. Lett. **107**, 272001 (2011).
 - [7] V.M. Abazov *et al.* (D0 Collaboration), Phys. Rev. Lett. **97**, 241801 (2006).
 - [8] P. Abreu *et al.* (DELPHI Collaboration), Eur. Phys. J. C **16**, 555 (2000); K. Ackerstaff *et al.* (OPAL Collaboration), Phys. Lett. B **426**, 161 (1998); D. Buskulic *et al.* (ALEPH Collaboration), Phys. Lett. B **377**, 205 (1996).
 - [9] F. Abe *et al.* (CDF Collaboration), Phys. Rev. D **59**, 032004 (1999).
 - [10] R. Aaij *et al.* (LHCb Collaboration), Phys. Rev. Lett. **112**, 111802 (2014); R. Aaij *et al.* (LHCb Collaboration), Phys. Lett. B **736**, 446 (2014).
 - [11] R. Aaij *et al.* (LHCb Collaboration), arXiv:1407.5873 [hep-ex], to appear in Phys. Rev. Lett.
 - [12] Charge conjugation is implied throughout this article.

- [13] V.M. Abazov *et al.* (D0 Collaboration), Nucl. Instrum. Methods Phys. Res. A **565**, 463 (2006).
- [14] J. Abdallah *et al.* (DELPHI Collaboration), Eur. Phys. J. C **32**, 185 (2004).
- [15] T. Sjöstrand *et al.*, Comput. Phys. Commun. **135**, 238 (2001). We use version 6.409.
- [16] D.J. Lange, Nucl. Instrum. Methods Phys. Res. A **462**, 152 (2001).
- [17] R. Brun *et al.*, CERN Report No. CERN-DD-EE-84-1 (1987).
- [18] J. Martínez Ortega, Ph. D. Thesis, Physics Department, CINVESTAV, Mexico City, November 2012 (unpublished), FERMILAB-THESIS-2012-60.
- [19] F. James and M. Roos, Comput. Phys. Commun. **10**, 343 (1975).
- [20] W. Verkerke and D. Kirkby, arXiv:physics/0306116.